Second-harmonic generation of I-III-VI_2 chalcopyrite semiconductors: Effects of chemical substitutions

Sergey N. Rashkeev[1] and Walter R. L. Lambrecht[2]
[1]*Department of Physics and Astronomy, Vanderbilt University, Nashville, Tennessee 37235*
[2]*Department of Physics, Case Western Reserve University, Cleveland, Ohio 44106-7079*
(Received 15 November 2000; published 6 April 2001)

We report first-principles calculations of the second-order optical response coefficients in the I-III-VI_2 (I=Ag,Cu; III=Ga,In; VI=S,Se,Te) chalcopyrite semiconductors. The computational approach uses the length-gauge formulation of perturbation theory which explicitly separates pure interband from mixed intraband-interband contributions. The expressions for static and frequency dependent second-harmonic generation coefficients are evaluated from band structures based on the local density approximation but including semiempirical gap corrections. The linear muffin-tin orbital method is used to calculate the required band structures and matrix elements. The results are in good agreement with experiment for the compounds for which data are available and provide predictions in the other cases. The trends show that the dominating factor determining $\chi^{(2)}$ is the anion rather than the group I or group III cation. The $\chi^{(2)}$ values clearly fall into separated groups with increasing value going from S to Se to Te. While this correlates approximately inversely with the band gap, several exceptions are notable: (1) Cu compounds have smaller gaps than corresponding Ag compounds and nevertheless have slightly lower $\chi^{(2)}$; (2) $AgGaTe_2$ has a higher gap than $AgInSe_2$ but nevertheless has a much higher $\chi^{(2)}$. An analysis of the various contributions to the frequency dependent imaginary part of the response functions, $\mathrm{Im}\{\chi^{(2)}(-2\omega,\omega,\omega)\}$, is presented in an attempt to correlate the $\chi^{(2)}$ values with band structure features. The main findings of this analysis are that (1) there is a large compensation between intra/inter- and interband contributions frequency by frequency as well as in the static values; (2) the static $\chi^{(2)}$ value is strongly affected by the sign of the low frequency parts of these separate contributions; (3) these low frequency parts correspond to only a few valence and conduction bands and only to so-called 2ω resonances; (4) the general shape of the $\mathrm{Im}\{\chi^{(2)}(-2\omega,\omega,\omega)\}$ response functions is determined by the band structures alone while the intensity, which ultimately explains the difference between tellurides and selenides, arises from the magnitude of the matrix elements. Starting from $AgGaSe_2$, the smaller effect on the $\chi^{(2)}$ due to In subsitution for Ga than to Te substitution for Se can be explained by the fact that the Ga to In substitution changes the gap only in a small region near the center of the Brillouin zone, while the Se to Te substitution changes the gap throughout the Brillouin zone. This shows that contributions from other parts of the Brillouin zone than the center dominate the behavior. The difference between Cu and Ag based compounds can be explained on the basis of a different degree of compensation of inter- and intra/interband contributions.

DOI: 10.1103/PhysRevB.63.165212 PACS number(s): 78.20.Bh, 42.65.Ky

I. INTRODUCTION

Ternary chalcopyrites are promising for optical frequency conversion applications in all solid state based tunable laser systems. These have potentially significant advantages over dye lasers because of their easier operation and the potential for more compact devices. Tunable frequency conversion in the midinfrared (IR) is based on optic parametric oscillators (OPO's) using pump lasers in the near IR.[1] On the other hand frequency doubling devices also allow one to expand the range of powerful lasers in the far infrared such as the CO_2 lasers to the midinfrared.[1,2]

The ternary chalcopyrite semiconductors come in two types: the II-IV-V_2 and I-III-VI_2 compounds, which are respectively derived from III-V and II-VI semiconductor compounds. While the binary semiconductors already allow for nonzero second-order response because of their lack of inversion symmetry, they are, with some exceptions, cubic and therefore optically isotropic. The distinct advantage of the chalcopyrites is their anisotropy, which leads to birefringence and hence allows for phase matching by angular tuning, i.e., by simply rotating the crystal orientation with respect to the optical beams. While some of the II-IV-V_2 compounds have higher $\chi^{(2)}$'s than the I-III-VI_2 compounds, (notably $CdGeAs_2$), they have typically smaller band gaps, being derived from less ionic III-V instead of II-VI compounds. This affects the high frequency limit of transparency and/or the types of laser that can be used to pump OPO's. Typically, one wants to stay significantly below the band gap for the pump laser to avoid two-photon and band tail absorption. Other differences result from the degree to which these materials can presently be purified and the degree of crystallographic perfection that can be achieved. Among the I-III-VI_2 chalcopyrites $AgGaS_2$ and $AgGaSe_2$ are the only ones that have so far been developed for use in frequency converting devices. While they do not offer the highest possible $\chi^{(2)}$'s among chalcopyrites, their wide range and superb degree of transparency and the range over which phase matching is possible are probably their greatest advantages. An overview of these materials' properties, crystal growth, unique advantages over other (say II-IV-V_2) chalcopyrites, and specific applications can be found in Ref. 2. The copper-

based compounds in the I-III-Vl_2 family, on the other hand, have been largely studied in view of their photovoltaic applications.[3–5]

In spite of the success some of the members of this family of compounds already enjoy, the properties of the entire family and the chemical trends are not yet well understood. The purpose of the present paper is to develop a better understanding of this interesting family of compounds. It complements our recent similar study of the II-IV-V_2 family.[6] This is important to guide further developments of new quaternary alloys with improved combinations of properties. As an example, it is of interest to develop compounds with so-called noncritical phase matching (NCPM) to optimize the frequency conversion for a specific frequency, for example, frequency doubling of CO_2 laser lines in the 9–11 μm range. Both $AgGa_xIn_{1-x}Se_2$ (Ref. 7) and $AgGaSe_{2x}Te_{2(1-x)}$ (Ref. 8) alloys have been suggested for this purpose. These possibilities are based on tuning the index of refraction to a desired value, making use of the fact that $AgGaSe_2$ is negative birefringent while the telluride and the In compound are positive birefringent. Note that NCPM for second-harmonic generation (SHG) is possible only in negative birefringent crystals and this is another possible advantage of the I-III-VI_2 family over the II-IV-V_2's. In a recent paper,[9] we have already pointed out the distinct advantage of the Te substitution versus the In subsitution approach because it has the beneficial side effect of much more strongly increasing $\chi^{(2)}$.

As a second example, $Cu_xAg_{1-x}GaS_2$ alloys have been shown to exhibit a significant band gap bowing,[10] with some intermediate compositions giving lower band gaps than the end compounds. Since $\chi^{(2)}$ is roughly inversely correlated to the band gap, one might think that this would lead to a possible route to further enhancement of $\chi^{(2)}$. However, as we shall see below, Cu compounds generally have lower $\chi^{(2)}$ than corresponding Ag compounds.

The important question related to the above observations of chemical trends is why? In other words, how are these trends reflected in the trends in the underlying electronic band structure? While we do not yet have complete answers to these questions, it is important first of all to establish the chemical trends clearly by studying not just isolated cases but the entire family of materials. In the present paper we systematically study the electronic structure and optical properties of a class of I-III-VI_2 ternary compounds with formula ABC_2 (A=Ag, Cu; B=Ga, In; C=S, Se, Te) which all exhibit the chalcopyrite crystal structure. Synthesis and crystal growth of new members of the family or mixed compounds to the point where reliable optical data can be obtained is time consuming. Therefore, a predictive computational approach as presented here should be of great value. Recently, we have shown that such a method is now available.[11,6] In the present paper, we will confirm again that good agreement is obtained between calculated and experimental values in the few cases where the experiments are available. Second, since our methodology is based on band structures, we attempt to provide an explicit link to the band structures and ask which band structure features are responsible for the trends obtained from the calculations. As we shall see, a rather complex interplay between various contributions occurs. This confirms our earlier observations on II-IV-V_2's.[6] On the other hand, the overall dominating chemical trend, namely, an increase in $\chi^{(2)}$ from S to Se to Te, will be shown ultimately to be due to a difference in momentum matrix elements.

The rest of the paper is organized as follows. In Sec. II we describe some details of our computational approach. In Sec. III we discuss the crystal structures and symmetry aspects of the $\chi^{(2)}$ tensors. In Sec. IV we show how we include gap corrections in the band structure in a semiempirical manner. In Sec. V we first present our calculated results for the static second-harmonic generation coefficients and discuss their trends. Next, we address the various questions raised in this Introduction by analyzing the results in terms of the decomposition of the frequency dependent $\mathrm{Im}\{\chi^{(2)}(-2\omega,\omega,\omega)\}$ function into intra- and interband terms as defined in Sec. II. Also, we compare different contributions using a band-to-band transition analysis. A summary of the main conclusions of this work is given in Sec. VI.

II. COMPUTATIONAL METHOD

The computational approach used in the present investigation was described in detail in our previous paper.[11] We use the so-called length-gauge formalism proposed by Sipe and co-workers.[12–14] This approach describes the interaction between the long-wavelength electromagnetic field and the solid in the form $e\mathbf{r}\cdot\mathbf{E}$, in which $\mathbf{r}$ is the position operator and $\mathbf{E}$ the electric field, instead of adding $-e\mathbf{A}/c$ to the momentum $\mathbf{p}$ operator with $\mathbf{A}$ the vector potential. In spite of the fact that the two Hamiltonians are equivalent through a unitary transformation there are several advantages in using the length-gauge formulation, namely, (i) the manifest absence of unphysical singularities in the zero-frequency limit without the need for invoking sum rules; (ii) the simple and natural account of the effects of the intraband motion of electrons which gives an essential contribution to the nonlinear optical (NLO) responses; (iii) explicit satisfaction of the Kleinman relations[15] in the zero-frequency limit. Moreover, this formalism allows one to extract the real singularities of the NLO responses that correspond to physical processes in the system (e.g., the current injection in a semiconductor irradiated by a circularly polarized light beam).[14]

The price one pays is that the matrix elements of the $\mathbf{r}$ operator between Bloch functions require care in their definition. Essentially, one has to use the crystal quasimomentum or $\mathbf{k}$ representation in which the $\mathbf{r}$ operator, acting on the coefficients of the expansion of an arbitrary wave function in the Bloch eigenfunctions of a given $\mathbf{k}$, is defined by[16]

$$\hat{\mathbf{r}} = i\nabla_{\mathbf{k}} + \hat{\Omega}, \tag{1}$$

with the $\hat{\Omega}$ operator defined in terms of its matrix elements between the periodic parts of the Bloch functions,

$$\langle i\mathbf{k}|\hat{\Omega}|j\mathbf{k}\rangle = \xi_{ij}(\mathbf{k}) = \frac{i(2\pi)^3}{\Omega_c}\int_{\Omega_c} u_i^*(\mathbf{k},\mathbf{r})\nabla_{\mathbf{k}} u_j(\mathbf{k},\mathbf{r})\, d^3r, \tag{2}$$

in which Ω_c is the volume of the unit cell. The main point, emphasized by Blount,[17] is that the diagonal elements ($i=j$) of $\hat{\Omega}$ are not well defined but their combination with the first term in Eq. (1), $i\nabla_{\mathbf{k}}$, is well defined. ''Well defined'' in the present context means independent of the arbitrary choice of the phase of the one-electron Bloch wave functions, which can be considered to be a gauge transformation. Thus, one arrives at a separation of the general $\mathbf{r}$ matrix elements between Bloch functions of different $\mathbf{k}$ and band index into an intraband and interband part:

$$\langle i\mathbf{k}|\mathbf{r}|j\mathbf{k}'\rangle = \langle i\mathbf{k}|\mathbf{r}_{inter}|j\mathbf{k}'\rangle + \langle i\mathbf{k}|\mathbf{r}_{intra}|j\mathbf{k}'\rangle,$$
$$= [1-\delta_{ij}]\,\delta(\mathbf{k}-\mathbf{k}')\,\xi_{ij}(\mathbf{k}) + \delta_{ij}[\,\delta(\mathbf{k}-\mathbf{k}')\,\xi_{ii}(\mathbf{k}) + i\,\delta(\mathbf{k}-\mathbf{k}')\nabla_{\mathbf{k}}]. \quad (3)$$

While the occurrence of a $\mathbf{k}$ gradient with a δ function may seem forbidding, it was shown by Aversa and Sipe[13] that the commutators one needs to calculate in practice are all fairly straightforward to evaluate. The use of this representation leads naturally to a decomposition of the nonlinear response into various terms related to intraband and interband matrix elements of the $\mathbf{r}$ operator. For example, the current operator also will have intra- and interband parts. An important point is that the density matrix ρ to first order in the perturbation has only an interband contribution but to second order has both intra- and interband contributions. Thus, in second order in the electric field, several mixed terms occur: a modification of the expectation value $\mathrm{Tr}\,\rho\mathbf{J}$ of the interband current operator due to the intraband parts of the density matrix, and terms arising from the intraband part of the current operator. In the following we refer to all but the pure interband term as ''intraband'' terms even though they are in fact mixed intra/interband terms. The pure interband term has the well-known form from molecular theories of second-order response,[18] if one considers the sum over $\mathbf{k}$ as simply a sum of independent contributions.

It should be mentioned that this approach neglects the excitonic and local-field effects. Unfortunately, there presently is no general formalism available to ascertain the errors made by making these approximations. Local-field effects have been studied by Levine and co-workers[19,20] but only in the nonadsorbing region. The effects were found to be of the order of 15% for the semiconductors under study and were found to reduce $\chi^{(2)}$. Excitonic effects on second-harmonic generation have been studied in the framework of the effective mass model for asymmetric superlattices by Atanasov *et al.*[21] and for superlattices with an applied electric field by Tsang and Chuang.[22] This work shows that SHG can be strongly enhanced at excitonic resonances, but this is essentially a result of the asymmetry in the envelope wave function and not related to the intrinsic bulk values that we are concerned with here. The methods used in those papers include only the specific quantum well derived SHG, not the bulk contribution, and thus only consider transitions between the few quantum well subbands and excitons derived from the bulk band edges. Tsang and Chuang found in their study that band-to-band contributions dominate the exciton derived contribution. To the best of our knowledge, a general *ab initio* formulation of second-harmonic generation including continuum and bound excitonic effects for a bulk material of arbitrary symmetry has not yet been given.

The general framework of our approach is thus second-order perturbation theory using the perturbation by the optical electric field written in the length gauge as mentioned above. There are two main approximations. First, we work within an effective independent particle model (specified by the local-density functional theory).[23] This means that excitonic effects and explicit exchange-correlation effects on the optical response functions are neglected but the exchange-correlation effects are included in the band structure taken as input in an averaged sense by the local-density approximation (LDA). The second main approximation is the long-wavelength limit, meaning that local-field effects are ignored. Our particular implementation of the method using the linear muffin-tin orbital band structure approach for band structures and matrix elements was presented previously[11] and was shown to give good agreement with a linear augmented plane wave (LAPW) implementation by Hughes and Sipe.[24] Our method has been successfully used for calculations of optical properties of SiC polytypes,[25] GaN-AlN superlattices,[26] $LiGaO_2$,[27] $ZnGeN_2$,[28] and, most relevant to the present paper, II-IV-V_2 chalcopyrites.[6]

The computational approach starts from the band structure calculated using the linear muffin-tin orbital (LMTO) method[29] in the atomic sphere approximation and with the potential determined as usual within the framework of density functional theory in the local-density approximation[23] but with an *a posteriori* self-energy correction applied to the gap, to be discussed in Sec. IV. The matrix elements required to calculate optical response are also calculated in a muffin-tin orbital basis set, in particular, using the one-center partial wave expansion of the wave functions. Angular momentum cutoffs and other convergence issues were discussed in Ref. 11. The integrations over the Brillouin zone (BZ) are performed using the tetrahedron method with well-converged $\mathbf{k}$-point meshes, typically corresponding to 256 points in the irreducible part of the BZ. Symmetrization of the integrands using the point group is used effectively while carrying out the integrations. For the ternary chalcopyrite semiconductors considered here, it was found that including the orbitals with angular moments $l_{max}=3$ in the basis set changes the results by a factor of 5–10 % at most. In most of our calculations we therefore include angular momenta up to $l_{max}=2$ only.

In order to facilitate the discussion of the band structure analysis to be presented below, in which we discuss various separate terms and contributions to $\chi^{(2)}(2\omega,\omega,\omega)$, we remind the reader of the final equations used to calculate SHG:[11]

$$\chi^{abc}_{inter}(-2\omega,\omega,\omega) = \frac{e^3}{\hbar^2\Omega}\sum_{cvn,\mathbf{k}}\frac{r^a_{vc}\{r^b_{cn}r^c_{nv}\}}{(\omega_{nv}-\omega_{cn})}\left[\frac{2f_{vc}}{\omega_{cv}-2\omega} + \frac{f_{nc}}{\omega_{nc}-\omega} + \frac{f_{vn}}{\omega_{vn}-\omega}\right], \quad (4)$$

in which $\{r^b_{ml}r^c_{ln}\}=(1/2)(r^b_{ml}r^c_{ln}+r^c_{ml}r^b_{ln})$ is a symmetrized combination of the dipole matrix elements $r^a_{nm}=\delta_{nm}p^a_{nm}/im\omega_{nm}$, which are in turn obtained from the momentum matrix elements p^a_{nm}. Superscripts (a,b,c) refer to the Cartesian coordinates. For the ''intraband'' contribution, one has

$$\chi^{abc}_{intra}(-2\omega,\omega,\omega)=\frac{i}{2}\frac{e^3}{\hbar^2\Omega}\sum_{cv,\mathbf{k}} f_{vc}\Bigg[\frac{2}{\omega_{cv}(\omega_{cv}-2\omega)}r^a_{vc}(r^b_{vc;c}+r^c_{cv;b})+\frac{1}{\omega_{cv}(\omega_{cv}-\omega)}(r^a_{vc;c}r^b_{cv}+r^a_{vc;b}r^c_{cv})$$
$$+\frac{1}{\omega^2_{cv}}\left(\frac{1}{\omega_{cv}-\omega}-\frac{4}{\omega_{cv}-2\omega}\right)r^a_{vc}(r^b_{cv}\Delta^c_{cv}+r^c_{cv}\Delta^b_{cv})-\frac{1}{2\omega_{cv}(\omega_{cv}-\omega)}(r^b_{vc;a}r^c_{cv}+r^c_{vc;a}r^b_{cv})\Bigg], \quad (5)$$

with the generalized **k**-space derivative

$$(r^b_{nm})_{;a}=\frac{r^a_{nm}\Delta^b_{mn}+r^b_{nm}\Delta^a_{mn}}{\omega_{nm}}+\frac{i}{\omega_{nm}}\sum_l(\omega_{lm}r^a_{nl}r^b_{lm}-\omega_{nl}r^b_{nl}r^a_{lm}), \quad (6)$$

in which $\Delta^a_{nm}=(p^a_{nn}-p^a_{mm})/m$ is the difference between two band velocities. We note that in the interband contribution three different states occur: c, the conduction, v, the valence, and n the intermediate band, which is either in the valence or in the conduction band. The sums are restricted to occupied or unoccupied bands by the Fermi factors such as $f_{vc}=f_v-f_c$ which, at zero temperature, are 1 if the band is occupied and 0 if the band is empty. In the mixed intra/interband term, only v and c, i.e., one interband transition, occur, but generalized derivatives given in terms of intraband velocities appear. These arise from the $\delta(\mathbf{k}-\mathbf{k}')\nabla_{\mathbf{k}}$ term in Eq. (3) and represent the intraband part of the electronic motion involvement. Ω is the normalization volume. We note that each term contains 2ω and ω resonances, corresponding to matching of either 2ω or ω to an interband transition. Each corresponding denominator is to be interpreted as having $\omega+i\delta$, and thus in the $\delta\rightarrow 0$ limit has an imaginary part that is a δ function joint density of states (JDOS) type of formula weighted by matrix element factors and a real part that is obtained from it by Kramers-Kronig transformation. We note that in general the static limit calculated directly is numerically consistent with the value obtained from the Kramers-Kronig transformation (the sum rule) within 5–10 % for all the cases studied here. The ''matrix element factors'' contain products of the pure momentum matrix elements and energy difference denominators, which influence the sign of each contribution.

While a simplified expression exhibiting this symmetry explicitly was derived in Ref. 11, it is useful to consider also the frequency dependent $\chi^{(2)}(-2\omega,\omega,\omega)$ even in the range above the band gap. The reason is that the imaginary part of this response function, $\mathrm{Im}\{\chi^{(2)}(-2\omega,\omega,\omega)\}$, from which the static value is obtained by a Kramers-Kronig transformation, can be analyzed in a manner similar to the imaginary part of the dielectric function $\epsilon_2(\omega)$ in terms of the underlying band structure. This should be clear from the above equations. A significant degree of cancellation among the interband and intra/interband contributions usually takes place. Thus an accurate calculation of all the terms is necessary to make reliable predictions and an analysis of these contributions may provide insights into the origins of $\chi^{(2)}$ enhancement in terms of the electronic band structure.

III. CRYSTAL STRUCTURES AND SYMMETRY CONSIDERATIONS

As already mentioned in the Introduction, the chalcopyrite structure with composition ABC_2 can be thought of as a particular ordered structure of the A and B cations on the cation sublattice of a zinc-blende structure with anion C. In particular, the II-IV-V_2 and I-III-VI_2 chalcopyrites can be obtained from the III-V and II-VI compounds, respectively, by replacing two group III (II) atoms per cell by II and IV (I and III) atoms. The crystal structure is a body-centered tetragonal lattice with eight atoms per unit cell. It can be thought of as a possibly tetragonally distorted A_2B_2 (or 2 + 2) face-centered cubic (fcc) superlattice in the {201} direction of the cations A and B with an interpenetrating distorted fcc lattice of common anions C displaced by $(1/4,u,c/8a)$. The cation ordering already breaks the cubic symmetry even if no distortion takes place but is then usually accompanied by some structural distortion as allowed by the new lowered symmetry. The structural parameters are the lattice constant a, which corresponds to the cubic lattice constant of the zinc-blende structure from which the chalcopyrite structure is derived, the ratio $\eta=c/a$, and the internal displacement parameter u. In the ideal structure $\eta=2$ and $u=1/4$. The nonideal value of u is due to the distortion of the anion sublattice, involving a shift by each anion away from one neighboring cation in the direction of another cation (of a different sort). The spacegroup is D^{12}_{2d} or $I\bar{4}2d$; the point group is D_{2d} or $\bar{4}2m$.

In the present work we preferred to use the available experimental values of the structural parameters a, η, and u instead of obtaining them by total energy minimization. The most complete set of parameters can be found in Refs. 30–32. A detailed discussion of the dependence of the band structure on the values of η and u, which characterize the distortion from the ideal chalcopyrite structure, can be found in our previous publication[6] for II-IV-V_2 materials.

Next, we discuss the tensorial aspect of $\chi^{(2)}$ for chalcopyrites. Because the point group is $\bar{4}2m$ there are only two independent components of the SHG tensor, namely, the 123 and 312 components (1, 2, and 3 refer to the x, y, and z axes,

TABLE I. Calculated LDA (E_g^{lda}) and experimental (Ref. 30) values of the energy gap (E_g^{expt}), measured and calculated values of the static $\chi^{(2)}$, and its decomposition in inter- and intraband contributions for different ternary semiconductors I-III-VI_2 (in pm/V).

Compound	E_g^{lda}	E_g^{expt} (eV)	$\chi^{(2)}_{expt}$	$\chi^{(2)}_{total}$	$\chi^{(2)}_{inter}$	$\chi^{(2)}_{intra}$
$AgGaS_2$	1.02	2.64	23 [a] 18 [b] 22 [c]	25.9	-24.1	50.0
$AgInS_2$	0.35	1.87		33.9	-39.0	72.9
$AgGaSe_2$	0.17	1.80	64 [a], 68 [b], 66 [c]	65.5	-7.6	73.1
$AgInSe_2$	0.10	1.24	72 [a], 63 [b]	83.3	-23.8	107.1
$AgGaTe_2$	0.17	1.32		138.0	-108.8	246.8
$AgInTe_2$	0.21	0.95		152.5	-157.7	310.2
$CuGaS_2$	0.92	2.43	19 [a], 14 [b]	22.7	-38.9	61.6
$CuInS_2$	0.01	1.53	14 [a], 11 [b]	31.7	-51.8	83.5
$CuGaSe_2$	0.20	1.68	57 [a], 44 [b]	55.5	-71.4	126.9
$CuInSe_2$	0.01	1.04		72.5	-115.0	187.5
$CuGaTe_2$	0.43	1.0 [d]–1.24		142.0	-186.8	328.8
$CuInTe_2$	0.18	1.06		126.0	-187.2	313.2

[a]Reference 30.
[b]Reference 37.
[c]Reference 36.
[d]The value used in the calculations is 1.0 eV.

respectively, which are chosen along the cubic axes).[18] With the usual matrix rather than third-rank tensorial notation, these are $\chi^{(2)}_{123}=2d_{14}$ and $\chi^{(2)}_{312}=2d_{36}$. In the static limit, these two components are equal according to the Kleinman ''permutation'' symmetry, which dictates additional relations between tensorial components beyond the purely crystallographic symmetry.

IV. GAP CORRECTIONS

It is well known that the LDA underestimates band gaps in semiconductors because the LDA Kohn-Sham states do not take into account the quasiparticle self-energy correctly. In particular, some of the compounds treated here have nearly vanishing gaps in the LDA, as can be seen from Table I. Under such circumstances, completely erroneous results would be obtained for $\chi^{(2)}$ because the latter is quite sensitive to the gap.

We have two semiempirical approaches at our disposal for correcting the gap: either simply adding a scissor shift, accompanied by a renormalization of the momentum matrix elements,[33,24,11] or adjusting certain potential parameters of the LMTO method.[11] As we argued previously,[11] the latter appears to provide better matrix elements for the transitions between the valence bands and the lowest conduction band because the eigenvectors are then changed consistently with the eigenvalues. Since the near gap transitions dominate the NLO response, as we will see below, the potential parameter adjustment approach is preferable.

In this approach, one adds semiempirical corrections to the diagonal elements of the LMTO Hamiltonian[11] to mimic the effect of state dependent and **k**-point dependent self-energy corrections. The approach is simply based on a general understanding of the predominant muffin-tin orbital character of the conduction band minima under consideration. For zinc-blende semiconductors, the main transitions between the valence and conduction bands at the Γ, X, and L points can be reasonably adjusted by shifting up the s orbitals for the cation and for the adjacent empty sphere (in the atomic sphere approximation). The states in chalcopyrite can be related to those in zinc blende by band structure folding arguments, explained, for example, in Ref. 35. The X point of zinc blende for example is folded to Γ and Z of chalcopyrite, whereas the L point of zinc blende is folded to X of chalcopyrite.

Some experimentation showed that shifting the Ag or Cu s states had little effect while shifting the Ga s or In s and the empty sphere s states nearest to those atoms did have an effect in opening the gap, while leaving the valence bands essentially unchanged. This indicates, as expected, the dominant role of the III cation s states in the lowest conduction band at Γ. Unfortunately, we do not have enough experimental information on the different band gaps in all chalcopyrites considered here. Instead of adjusting each compound individually, we decided it was preferable to treat the shifts as transferable parameters representative of the atom. We first adjusted the gaps at the three **k** points mentioned earlier for the zinc-blende II-VI compounds CdS, CdSe, CdTe, ZnS, ZnSe, and ZnTe to those obtained in GW quasiparticle calculations.[34] These showed only slight differences between the shifts for Cd and Zn for the different compounds. We thus used the same shift for Ga s and In s states, and nearly constant values for the shifts throughout the series of compounds, and adjusted the remaining discrepancies by means of a constant shift or scissor correction. The potential parameter shift values were chosen to open the gap at least about halfway so as to avoid the wrong LDA band masses in cases of nearly zero gap. We used only about half the values of the shifts in II-VI compounds to make sure no gaps were overcorrected, keeping in mind that we would adjust the remainder with an unbiased scissor correction.

In part, the smaller gaps in I-III-VI_2 compounds than in the corresponding II-VI compounds is due to the fact that the Ag and Cu d-bands are closer to the valence band than are the Cd d or Zn d bands. While the Cd $4d$ bands lie at about -7.5 eV below the valence band maximum in the LDA, the Ag $4d$ bands lie near -4.0 eV and hybridize significantly with the S, Se, or Te p bands. The Cu $3d$ bands lie between -2 and -4 eV while the Zn $3d$ bands lie at about -6.5 eV. This tends to push up the valence band and thus reduce the gap.

To finish this section on band gaps, we note that all the I-III-VI_2 materials considered have a direct band gap with the minimum at the Γ point. This is different from the case of II-IV-V_2 chalcopyrites considered in our previous paper,[6] where the band gap varies from direct to pseudodirect or indirect.

V. RESULTS

A. Trends in static values

Table I provides our results for the static (zero-frequency) values of the SHG as well as intra- and interband contributions along with the values of the gaps discussed before.

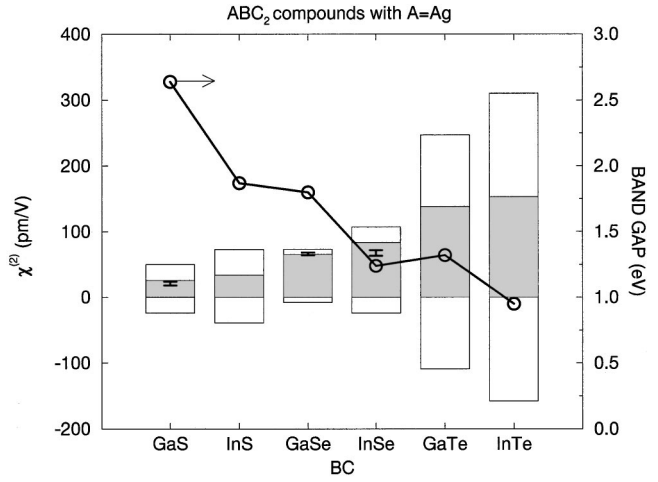

FIG. 1. Static $\chi^{(2)}$ values for ABC_2 compounds (A=Ag, B=Ga, In; C=S, Se, Te). Positive bars, intraband contribution; negative bars, interband contribution; shaded area, total value. The experimental values of the direct gap from Ref. 30 are shown by circles with scale on the right. The error bars show the minimal and maximal experimental values of SHG from Refs. 30 and 37.

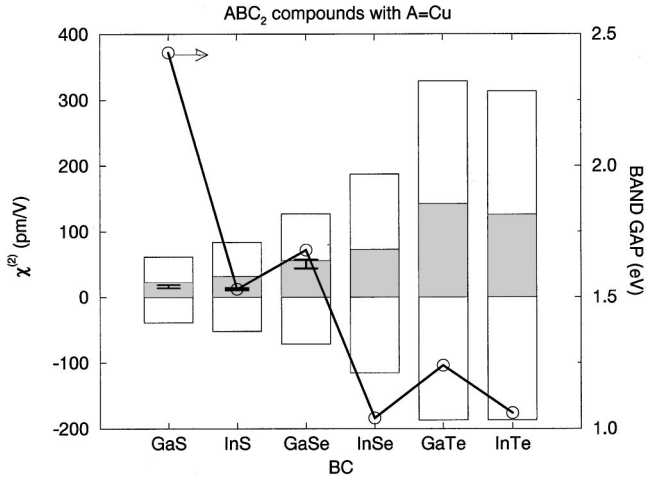

FIG. 2. Static $\chi^{(2)}$ values for ABC_2 compounds (A=Cu; B=Ga, In; C=S, Se, Te). The symbols are the same as in Fig. 1.

The total SHG values are seen to be in good agreement with experimental ones where the experiment is available with the exception of $CuInS_2$.[36,30,37] Clear chemical trends are apparent. There is a general tendency toward higher $\chi^{(2)}$ from Ga to In and from S to Se to Te. However, the most important factor is clearly the anion. The Ga to In change gives only a modest increase of about 10-30 %, while the S to Se and Se to Te changes are by a factor of 2 or more. This fact is interesting for practical applications. In particular, the values in the tellurides become competitive with those of the II-IV-V_2 chalcopyrites, for example, larger than $\chi^{(2)}$ in $ZnGeP_2$. It is also noteworthy that at the same time the band gaps stay near or above 1 eV. Thus the increase in $\chi^{(2)}$ is not at the expense of a reduced frequency range. Also, the index of refraction is not too much affected by going from selenides to tellurides. The actual figure of merit for frequency conversion applications, $[\chi^{(2)}]^2/n^3$, is thus even more strongly enhanced than is $\chi^{(2)}$ itself.

If we compare these results to the known values of $\chi^{(2)}$ in II-VI compounds we see that the enhancement of the SHG when one substitutes Se by Te is less dramatic—$\chi^{(2)}(0)$ = 30, 80, and 90 pm/V for zinc-blende ZnS, ZnSe, and ZnTe and 40, 50, and 60 pm/V for zinc-blende CdS, CdSe, and CdTe, respectively. For CdS and CdSe the 123 component for the zinc-blende structure has been calculated from the 333 component of the wurtzite phase, the actual structure in which these materials occur,[37] using simple geometric relations among the tensor components.[25] Thus, the strong enhancement of the SHG in the I-III-VI_2 materials by a factor of 2 with each anion substitution is rather surprising. The reason for this difference from the II-VI's will require further study of the II-VI NLO response. Here we restrict the discussion to the I-III-VI_2 materials.

The compensation between the interband and intraband terms can be analyzed from Table I and Figs. 1 and 2. For all the materials considered the interband contribution is negative, while the intraband one is positive, and there is a significant compensation between them. It is noteworthy though that in the silver selenides this compensation is the smallest, i.e., the interband term is very small. This situation resembles that of $CdGeAs_2$ in the II-IV-V_2's,[6] where the absence of compensation between the intraband and interband contributions gives rise to its record SHG coefficient (about 500 pm/V). In copper selenides, however, the compensation is ''normal,'' and the interband contribution is comparable with the intraband one. In spite of the very low compensation in silver selenides, the absolute value of the intraband term in these materials is still lower than in the tellurides. This is true for both the compounds of silver and copper.

Generally speaking, we also see an increase from Ga to In with the only exception that SHG in $CuGaTe_2$ is a little higher than in $CuInTe_2$. However, this effect is smaller than the effect of the anion substitution.

The trend in $\chi^{(2)}$ is seen to be inversely correlated with the gaps in an overall sense. This is most clearly seen in Fig. 3 which shows a clear separation of all tellurides from se-

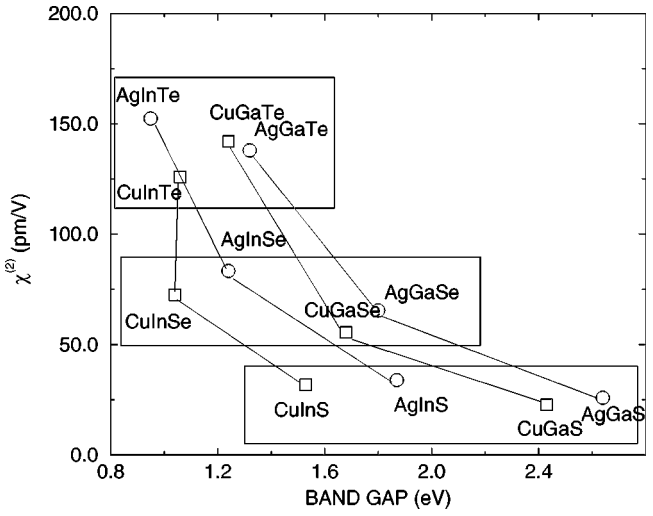

FIG. 3. Static $\chi^{(2)}$ values versus gap for various compounds.

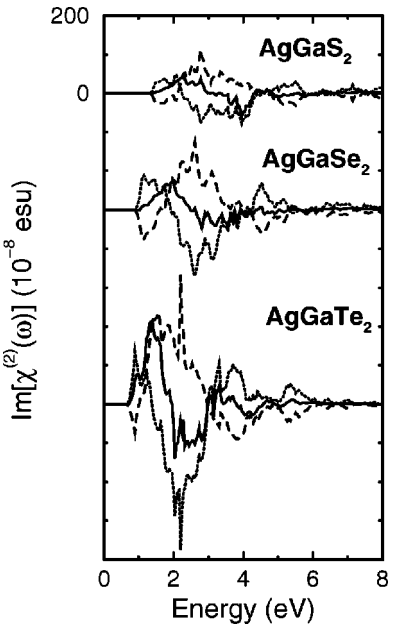

FIG. 4. Frequency dependent $\mathrm{Im}[\chi^{(2)}(-2\omega,\omega,\omega)]$ for $AgGaS_2$, $AgGaSe_2$, and $AgGaTe_2$ as function of energy $\hbar\omega$. Solid line, total; dotted line, interband; dashed line, intraband contribution. The curves for $AgGaSe_2$ and $AgGaTe_2$ were shifted down by an arbitrary amount.

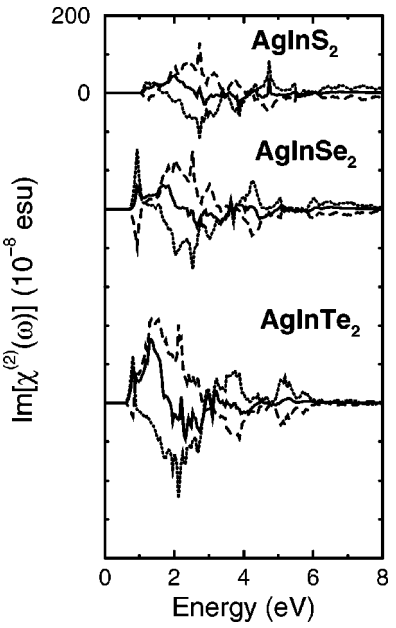

FIG. 5. Frequency dependent $\mathrm{Im}[\chi^{(2)}(-2\omega,\omega,\omega)]$ for $AgInS_2$, $AgInSe_2$, and $AgInTe_2$ as function of energy $\hbar\omega$. Solid line, total; dotted line, interband; dashed line, intraband contribution.

lenides and sulfides. However, for compounds with nearly the same gap, the rule cannot be used to predict which material will have the largest $\chi^{(2)}$. For example, going from $AgGaSe_2$ to $AgGaTe_2$ decreases the gap slightly less than by going to $AgInSe_2$, but the SHG coefficient increases far more for the Te substitution than for the In substitution. Also, we find systematically that the Cu compounds have smaller gaps than the corresponding Ag compounds, and yet have a smaller $\chi^{(2)}$. Thus, the inverse correlation with gaps that has been emphasized before[38] provides only a rough guideline but not a precise predictive tool.

B. Frequency dependent response

In order to better understand the origin of the relative magnitudes of the intra- and interband contributions, we now consider the frequency dependent $\chi^{(2)}$ functions, or, more precisely, their imaginary part $\mathrm{Im}[\chi^{(2)}(-2\omega,\omega,\omega)]$ (we also use the simplified notation $\mathrm{Im}[\chi^{(2)}(\omega)]$), from which the real part and in particular its static value can be obtained by a Kramers-Kronig transformation. Figures 4–7 show the imaginary part of the frequency dependent $\chi^{(2)}(\omega)$ for the 123 components in all the I-III-VI_2 materials considered. In these figures, the horizontal axis corresponds to $\hbar\omega$. Also, we show the frequency dependent interband and intraband parts for all of them. One may note that the overall shape of the SHG curves for all materials considered is rather similar. Yet, some of the fine structure details will be shown to play a role in understanding the trends in the static values.

First, we note the opposite signs of both contributions throughout the frequency range. We now consider the Kramers-Kronig integral

$$\mathrm{Re}[\chi^{(2)}(0,0,0)] = (2/\pi)\mathcal{P}\int_0^\infty \{\mathrm{Im}[\chi^{(2)}(-2\omega,\omega,\omega)]/\omega\}d\omega \tag{7}$$

of these separate contributions to derive the static low frequency limit. Clearly, this integral will emphasize the low frequency region. At energies higher than 5 eV the imaginary part of SHG drops to zero very fast.

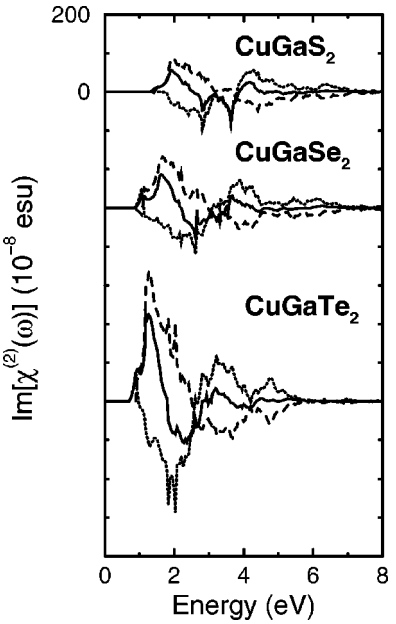

FIG. 6. Frequency dependent $\mathrm{Im}[\chi^{(2)}(-2\omega,\omega,\omega)]$ for $CuGaS_2$, $CuGaSe_2$, and $CuGaTe_2$ as function of energy $\hbar\omega$. Solid line, total; dotted line, interband; dashed line, intraband contribution.

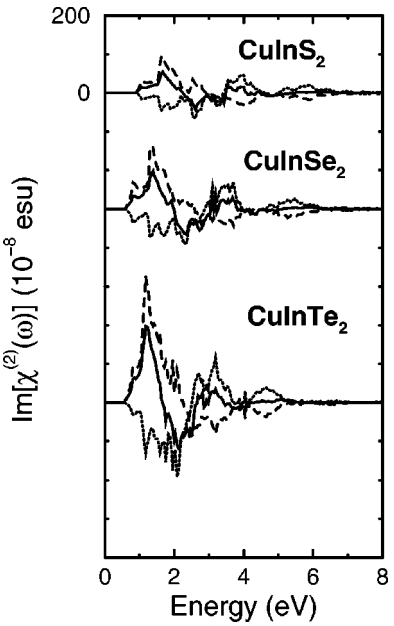

FIG. 7. Frequency dependent $\mathrm{Im}[\chi^{(2)}(-2\omega,\omega,\omega)]$ for $CuInS_2$, $CuInSe_2$, and $CuInTe_2$ as function of energy $\hbar\omega$. Solid line, total; dotted line, interband; dashed line, intraband contribution.

The interband contribution in the AgGa-VI_2 series (Fig. 4) starts off with a positive peak, then becomes negative, and then swings to positive again. In view of the Kramers-Kronig emphasis on the low energy region, this is significant. The curve giving the total contribution to $\chi^{(2)}$ for these materials shows that, even though there is a significant negative contribution between about 2 and 3 eV, the large first positive peak dominates. Taking into account the energy denominator weight factor in the Kramers Kronig transformation, we can understand that the net interband contribution is strongly suppressed by this sign change. Comparing the areas under the curve between first (positive) and second (negative peak) in the interband spectrum, we can see that the largest degree of compensation is expected in the Se compound. This is consistent with what we noticed earlier, namely, that the interband contribution to the static value is smallest in the two Ag based Se compounds, and in particular in $AgGaSe_2$. The same discussion applies to some extent to $AgInSe_2$.

Comparing In to Ga compounds, we notice that the first positive peak in the interband contribution becomes very narrow, i.e., less significant in weight. Also, in $AgGaTe_2$, the area under the first positive peak in the interband contribution is significantly smaller than the area of the subsequent negative peak, thus leading to a more negative overall contribution to the interband static value and a larger degree of compensation of inter- and intraband contributions.

Next, comparing Cu based to Ag based compounds, we note that the first positive peak is almost completely absent, except in $CuGaSe_2$ and $CuGaTe_2$, in which cases they are still very small. Thus, in all Cu compounds, the interband contribution is strongly negative. In fact, comparing corresponding Ag and Cu compounds, we note a stronger negative interband contribution in the Cu compounds. For example, comparing $AgGaSe_2$ with $CuGaSe_2$, we can see that while the intraband contribution is actually larger in $CuGaSe_2$ the total value is nevertheless smaller than in the Ag compound because of the much stronger negative interband contribution. Thus, we can state that to some extent the lower $\chi^{(2)}$ values of Cu versus Ag compounds in spite of having smaller gaps are related to the larger degree of compensation of intraband by interband contributions.

Next, we compare overall intensities of features. Here we see a clear trend of increasing absolute value of all spectral features from S to Se to Te. So, while the differences between Ga and In and Cu vs Ag are affected strongly by the interplay of inter- and intraband contributions, the most obvious trend of $\chi^{(2)}$ static values appears to result from overall intensities of both types of contribution.

Overall, we learn from this that (1) interband/intraband differences play a role in the effects of Ga to In and Cu to Ag substitution, but (2) it is the overall increase in intensity of all contributions in the case of tellurides that leads to it having the largest $\chi^{(2)}$ rather than the subtleties of intra/interband cancellations; and (3) it is the low energy region below 2–3 eV that dominates the behavior in these materials.

To gain further insights into the band structure origins of the $\chi^{(2)}$ trends, we now turn to a more detailed analysis of the low energy portions of the nonlinear response functions. It is well known that the SHG spectra are more sensitive to fine details of the crystal and the underlying band structure than the corresponding linear response functions. There are two main reasons for that sensitivity. For one thing, the second-order response involves more ''resonances'' than the linear one. In addition to the usual ω resonances there appear the 2ω resonant contributions; see Sec. II. Secondly, the real and imaginary parts of the products of matrix elements, which control the strength of a given resonance in $\chi^{(2)}$, can be positive or negative. In contrast, for the linear responses the corresponding factors involve only the square of matrix elements, which ensures, for example, that $\varepsilon_2(\omega)$ is positive. As a result, the structure in $\chi^{(2)}(-2\omega,\omega,\omega)$ is more pronounced than in the linear response. The question now is which of these factors has the dominant effect.

Figure 8 shows an example of such an ω vs 2ω analysis of resonant contributions to $\mathrm{Im}[\chi^{(2)}(\omega)]$. It can be shown that the low energy region is dominated by the ''2ω'' resonances for all the materials considered. This is a quite generally true[11,6] and happens because the direct transition threshold for the 2ω part occurs at an energy that is half that for the ω part, i.e., near the threshold the 2ω contribution is the only one that exists.

In addition to ω vs 2ω analysis one can analyze different terms in SHG by a decomposition into separate band-to-band contributions, similar to the well-known way of analyzing linear optical response. Figure 9 shows that the dominating low energy peak in SHG, which plays a crucial role in the formation of the zero-frequency value of $\chi^{(2)}$, originates from the 2ω term and is due to the transitions from the three upper valence to the two lower conduction bands.

This fact significantly simplifies the electronic structure interpretation of the frequency dependent SHG because we have to focus on only a few bands near the gap. For example, we now consider the following question: Starting from

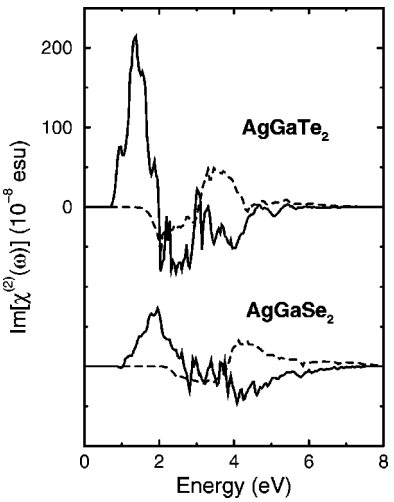

FIG. 8. Frequency dependent 2ω (solid line) and ω (dashed line) contributions to the total Im[$\chi^{(2)}$] for $AgGaTe_2$ and $AgGaSe_2$ as function of $\hbar\omega$.

$AgGaSe_2$, why does Te subsitution for Se increase the susceptibility more than In substitution for Ga, in spite of the fact that the latter decreases the gap more?

Let us inspect the electronic band structures for $AgGaTe_2$, $AgGaSe_2$, and $AgInSe_2$ (Fig. 10). We note that, whereas $AgInSe_2$ has a reduction of the gap relative to $AgGaSe_2$ only near the Γ point, $AgGaTe_2$ exhibits an overall reduction of the gap over the entire Brillouin zone. This is at least suggestive that the reason why $\chi^{(2)}$ in $AgInSe_2$ is not as much increased as in $AgGaTe_2$ might be due to the fact that the region around Γ does not make a sizable contribution to $\chi^{(2)}$. Also, the upper valence and lower conduction bands in

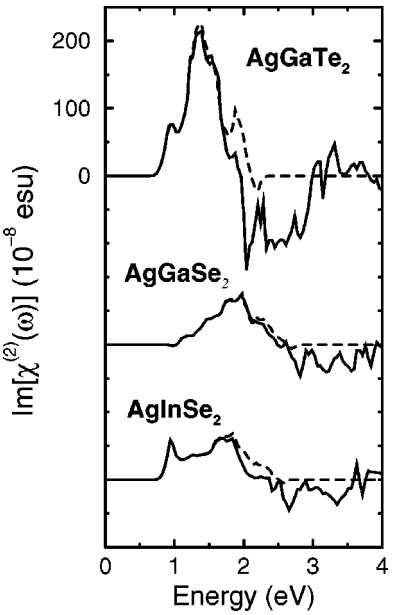

FIG. 9. Frequency dependent total Im[$\chi^{(2)}$] (solid line) and the contribution from the transitions between the three upper valence and the two lower conduction bands to the 2ω term (dashed line) for $AgGaTe_2$, $AgGaSe_2$, and $AgInSe_2$ as function of $\hbar\omega$.

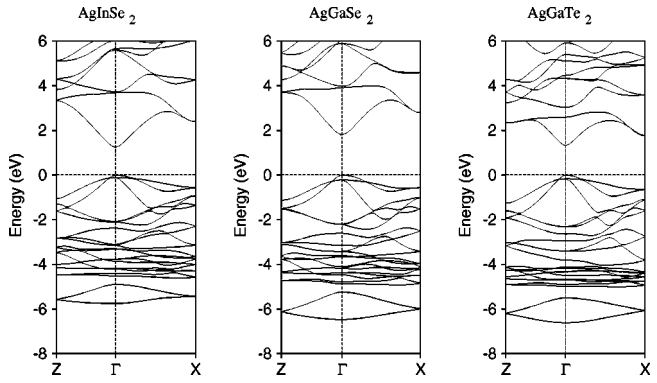

FIG. 10. Electronic bands of $AgInSe_2$, $AgGaSe_2$, and $AgGaTe_2$, including semiempirical gap correction, along the Z-Γ and Γ-X lines in the Brillouin zone [$Z=(2\pi/\eta a)(0,0,1)$; $\Gamma=(0,0,0)$; $X=(2\pi/a)(1/2,1/2,0)$] for the experimental crystal structure. The energy reference is at the top of the valence band.

$AgGaTe_2$ seem to be more ''parallel,'' i.e., the difference of curvature between them is lower than in $AgGaSe_2$. This gives an additional amplifying factor when one takes the integrals over the Brillouin zone, making the oscillator strength of all the peaks bigger. This clearly shows that trends in $\chi^{(2)}$ cannot be based solely on the minimum band gap. In fact, it indicates that the ''average'' band gap plays a more significant role.

This difference in the gap behavior between the two materials can be explained by the fact that the conduction band minimum at Γ has strong cation s character whereas other states in the conduction band are more heavily mixed with other atomic orbitals such as anion p states. The overall reduction in gap by substitution of Se by Te is consistent with an overall weakening of the bonds, and, therefore, with a smaller bonding-antibonding splitting. Fortunately, it does not affect the short-wavelength cutoff significantly, so that the usual laser pumps for OPO's can still be used. On the other hand, the weakening of the bonds and the heavier Te atom may be expected to push the multiphonon absorption edge slightly further toward longer wavelengths. Weaker bonds and a heavier atom (Te instead of Se) will lead to lower phonon frequencies. In particular, as is already the case in $AgGaSe_2$, it lies beyond the CO_2 laser lines,[8] which is of practical significance for the intended applications of these materials.

Up to this point, we have argued that the differences between various compounds in this family can be related to the interplay of inter- and intraband contributions, and the latter to the behavior of only a few bands near the gap. However, in order to understand the most obvious trend from S to Se to Te, these considerations are not sufficient. Ultimately, this trend appears to arise from the simple fact that both intra- and interband parts of the spectra have higher overall intensities in Te than in Se than in S compounds.

A lower average gap implies smaller factors such as $(\omega_{cv}-2\omega)^{-1}$ in Eqs. (4) and (5). One might expect that this would increase the intensity of the spectral features in both the inter- and intraband contributions. We have already explained that In substitution has only a minor effect because it

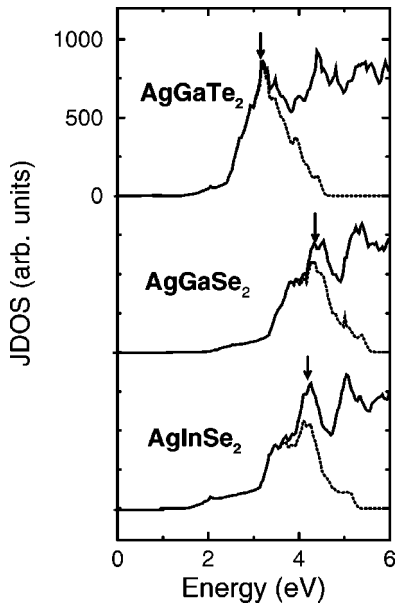

FIG. 11. JDOS's for $AgGaTe_2$, $AgGaSe_2$, and $AgInSe_2$ (solid line), and the partial contribution from the transitions between the thre upper valence and two lower conduction bands (dotted line).

affects the gap only near the center of the BZ. But can the intensity difference of the spectral features be explained completely in terms of the size of the average energy transition denominators? We now show that in fact it cannot. This suggests that ultimately matrix elements, which characterize the wave functions of the upper valence and the lower conduction band states, are responsible for this trend.

Figure 11 shows the joint density of states for the same three materials shown in Fig. 9. In general, the JDOS has the same features as the linear response function. Its peaks correspond to the transitions with high oscillator strength. This transitions occur in the regions of the **k** space where the corresponding pair of bands has a small difference in curvature, i.e., they are nearly parallel. However, the JDOS completely ignores the optical transition matrix elements, which are equal to zero if the transition is forbidden by, e.g., a symmetry argument. Figure 11 shows that in spite of the fact that the bands are more ''parallel'' in $AgGaTe_2$ than in the two other materials this factor is actually not all that important. For the transitions between the three upper valence and two lower conduction bands (which accounts almost entirely for the zero-frequency SHG), the oscillator strength changes by a factor of only 1.3 when one goes from $AgGaTe_2$ to $AgGaSe_2$.

Even more instructive is the calculated value of the 2ω term of the SHG under the assumption that the momentum matrix elements are equal to unity (Fig. 12). This quantity corresponds to SHG in the same way in which the JDOS corresponds to the imaginary part of the dielectric function. These curves clearly show that the amplitudes of this function is even more independent of the material than is the JDOS. This means that the analysis of densities of states is not enough, and one should take into account the momentum matrix elements of the electronic transitions to understand the differences in $\chi^{(2)}$.

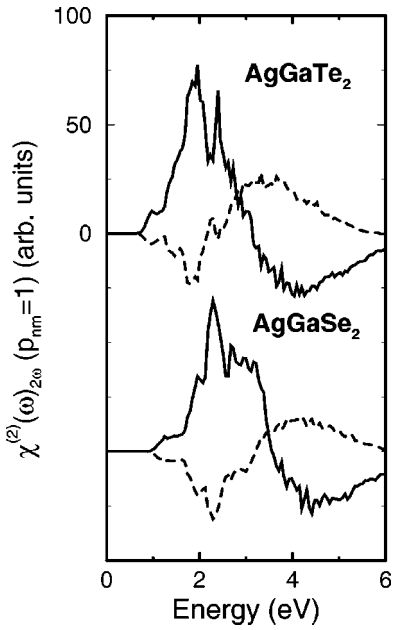

FIG. 12. The 2ω resonant contribution to SHG for $AgGaSe_2$ and $AgGaTe_2$ as function of $\hbar\omega$, calculated in the approximation that all the momentum matrix elements are equal to unity: interband term, solid line; intraband term, dashed line.

At the same time, it is interesting to observe that the overall shape of the spectral function that we discussed above, namely, a positive peak in interband contribution at low energies, followed by a negative peak, and then again a positive peak, is maintained even if we set all matrix element equal. This shows that it is not the sign changes of the momentum matrix elements products as such but rather the prefactors containing energy band differences that lead to this overall behavior. With reference to Eqs. (4) and (5), we note that all terms have the general structure of a $(\omega-\omega_{ij})^{-1}$ denominator, a momentum matrix element combination, and additional factors containing energy band differences such as $\omega_{cv}=\omega_c-\omega_v$. It is clear that these last factors are responsible for the sign changes.

At the present moment we do not have a good physical explanation of what determines the relative magnitudes of the momentum matrix elements of sulfides, selenides, and tellurides, but apparently their difference is what ultimately underlies the main trend in $\chi^{(2)}$ values.

VI. CONCLUSIONS

In summary, we have presented a systematic and comprehensive investigation of the frequency dependent and static second-harmonic generation response functions of the I-III-VI_2 chalcopyrites (with I=Ag or Cu, II Ga or In, and VI=S, Se, or Te) based on first-principles calculations of the electronic band structure and optical matrix elements. The only parameter that was adjusted to experiment in the band structures used as input in the $\chi^{(2)}$ calculations is the band gap. Good agreement was obtained with experiment for the few compounds for which data are available. For the other compounds our results stand as predictions to be verified.

The clearest trend obtained from our calculations is an increase in $\chi^{(2)}$ from S to Se to Te compounds. This trend, as expected, is correlated inversely with the band gap. Still, various aspects are somewhat unexpected. The increase in $\chi^{(2)}$ from S to Se to Te is much larger in I-III-VI_2 compounds than in II-VI's. While the Cu compounds have systematically smaller gaps than the Ag compounds they have lower rather than higher $\chi^{(2)}$. Ga to In subsitution generally increases $\chi^{(2)}$ but only slightly. Also, while $AgInSe_2$ has a smaller gap than $AgGaTe_2$, the telluride has a significantly higher $\chi^{(2)}$.

Our analysis identified the dominant contributions to the static $\chi^{(2)}$ in terms of the Kramers-Kronig transformation of the contributions to the $\mathrm{Im}\{\chi^{(2)}(-2\omega,\omega,\omega)\}$ functions. In all cases, the low energy region of the latter gives the dominant contribution, in which so-called 2ω resonances are the only or at least the most important contribution. Further analysis showed that only a few valence and conduction bands near the fundamental gap influence this energy region. Some of the discrepancies from the general rule of thumb of increasing $\chi^{(2)}$ with decreasing gap can be traced back to the behavior of the interband contribution in the low energy region. If this function has a sign change in the low energy region, a significant cancellation of the contributions below and above the node can lead to a very small negative pure interband contribution. This circumstance is favorable for a high $\chi^{(2)}$ because then the mixed intra/interband contribution, which is positive in these compounds, dominates. This occurs, for instance, most strongly in the Ag-III-Se_2 compounds. It occurs to some degree in all Ag compounds but more markedly in the Ga than in the In compounds. It does not occur in the Cu-derived compounds, which thereby end up with slightly lower $\chi^{(2)}$ than their Ag based counterparts. It was further found that this overall spectral shape of the functions is to a large extent determined by the band structure itself. It was maintained even if momentum matrix elements were taken as constant showing that it does not occur because of a change in momentum matrix element products.

In part the differences between $AgGaTe_2$ and $AgInSe_2$ could be related to the fact that in the latter the gap is reduced from that of $AgGaSe_2$ only near the Γ point, which does not give a dominant contribution to $\chi^{(2)}$, while in the former the gap is reduced throughout the BZ. This feature explains why the lower gap in $AgInSe_2$ does not necessarily lead to a higher $\chi^{(2)}$.

On the other hand, it was found that the overall change in intensity of the spectral features from S to Se to Te, which ultimately is responsible for the trend of the static values, depends crucially on including the proper matrix elements. In other words, it is the size of these matrix elements that is responsible for the dominant trend in these materials.

Since at this point no experimental values are available for the $\chi^{(2)}$ tellurides and our calculations predict a significant advantage for these materials[9] we hope our work will stimulate further experimental efforts on these materials. On the theory side, a more *ab initio* treatment of the quasiparticle gap corrections is desirable and considered to be a priority for future work. More detailed experimental information on the band structures of these compounds, for example, from UV reflectivity measurements or angular resolved photoemission, will be useful for further refining these predictions.

ACKNOWLEDGMENT

This work was supported by the Air Force Office of Scientific Research under Grant No. F49620-00-1-0037.

[1] F. K. Hopkins, Laser Focus World **31**, 87 (1995).
[2] G. C. Catella and D. Burlage, MRS Bull. **23**, 28 (1998), and other papers in the same volume.
[3] G. D. Boyd, H. Kasper, and J. H. McFee, IEEE J. Quantum Electron. **7**, 563 (1971).
[4] A. M. Gabor, J. R. Tuttle, D. S. Albin, M. A. Contreras, R. Noufi, and A. M. Hermann, Appl. Phys. Lett., **65**, 198 (1991).
[5] J. Hedstrom, H. Ohlsen, M. Bodegard, A. Kylner, L. Stolt, D. Hariskos, M. Ruckh, and H. W. Schock, in *Proceedings of the 23rd IEEE Photovoltaic Specialist Conference*, (IEEE, New York, 1993), p. 364.
[6] S. N. Rashkeev, S. Limpijumnong, and W. R. L. Lambrecht, Phys. Rev. B **59**, 2737 (1999).
[7] G. C. Bhar, S. Das, U. Chatterjee, P. K. Datta, and Yu N. Andreev, Appl. Phys. Lett. **63**, 1316 (1993).
[8] M. C. Ohmer, J. T. Goldstein, D. E. Zelmon, A. W. Waxler, S. M. Hegde, J. D. Wolf, P. G. Schunemann, and T. M. Pollak, J. Appl. Phys. **86**, 94 (1999).
[9] S. N. Rashkeev and W. R. L. Lambrecht, Appl. Phys. Lett. **77**, 190 (2000).
[10] In-Hwan Choi, Sung-Hwan Eom, and P. Y. Yu, J. Appl. Phys. **87**, 3815 (2000).
[11] S.N. Rashkeev, W.R.L. Lambrecht, and B. Segall, Phys. Rev. B **57**, 3905 (1998).
[12] J. E. Sipe and E. Ghahramani, Phys. Rev. B **48**, 11 705 (1993).
[13] C. Aversa and J.E. Sipe, Phys. Rev. B **52**, 14 636 (1995).
[14] J. E. Sipe and A. I. Shkrebtii, Phys. Rev. B **61**, 5337 (2000).
[15] D.A. Kleinman, Phys. Rev. **126**, 1977 (1962).
[16] E. M. Lifschitz and L. P. Pitaevskii, in *Statistical Physics, Part 2*, Vol. 9 of *Landau and Lifschitz Course of Theoretical Physics* (Pergamon Press, Oxford, 1980), Chap. VI, p. 223.
[17] E. I. Blount in *Solid State Physics, Advances in Research and Applications*, edited by F. Seitz and D. Turnbull (Academic, New York, 1962) Vol. 13, p. 305.
[18] R. W. Boyd, *Nonlinear Optics* (Academic Press, Boston, 1992).
[19] Z. H. Levine, Phys. Rev. B **42**, 3567 (1990); Z. H. Levine and D. C. Allan, *ibid.* **44**, 12 781 (1991); Z. H. Levine, *ibid.* **49**, 4532 (1994).
[20] J. Chen, L. Jönsson, J. W. Wilkins, and Z. H. Levine, Phys. Rev. B **56**, 1787 (1997).
[21] R. Atanasov, F. Bassani, and V. M. Agranovich, Phys. Rev. B **50**, 7809 (1994).
[22] L. Tsang and S.-L. Chuang, Phys. Rev. B **42**, 5229 (1990).
[23] P. Hohenberg and W. Kohn, Phys. Rev. **136**, B864 (1964); W.

Kohn and L. J. Sham, *ibid.* **140**, A1133 (1965).
[24] J. L. P. Hughes and J. E. Sipe, Phys. Rev. B **55**, 13 630 (1997); **53**, 10 751 (1996).
[25] S. N. Rashkeev, W. R. L. Lambrecht, and B. Segall, Phys. Rev. B **57**, 9705 (1998).
[26] S. N. Rashkeev, W. R. L. Lambrecht, and B. Segall, in *Nitride Semiconductors*, edited by F. A. Ponce, S. P. DenBaars, B. K. Meyer, S. Nakamura, and S. Strite, Mater. Res. Soc. Symp. Proc. **482** (Materials Research Society, Pittsburgh, 1998), p. 857.
[27] S. N. Rashkeev, S. Limpijumnong, and W. R. L. Lambrecht, J. Opt. Soc. Am. B **16**, 2217 (1999).
[28] S. Limpijumnong, S. N. Rashkeev, and W. R. L. Lambrecht, MRS Internet J. Nitride Semicond. Res. **4S1**, G6.11 (1999).
[29] O. K. Andersen, Phys. Rev. B **12**, 3060 (1975); O. K. Andersen, O. Jepsen, and M Šob, in *Electronic Band Structure and its Applications*, edited by M. Yussouf (Springer, Heidelberg, 1987), p. 1.
[30] J. L. Shay and J. H. Wernick. *Ternary Chalcopyrite Semiconductors: Growth, Electronic Properties, and Applications* (Pergamon Press, Oxford, 1975).
[31] R. W. G. Wyckoff, *Crystal Structures* (Interscience Publishers, New York, 1963).
[32] A. MacKinnon, in *Numerical Data and Functional Relationships in Science and Technology*, edited by O. Madelung, Landolt-Börnstein, New Series, Group III, Vol. 17, Pt. h (Springer, Berlin, 1985), p. 9.
[33] Z. H. Levine and D. C. Allan, Phys. Rev. Lett. **63**, 1719 (1989).
[34] O. Zakharov, A. Rubio, X. Blase, M. L. Cohen, and S. G. Louie, Phys. Rev. B **50**, 10 780 (1994).
[35] S. Limpijumnong, W. R. L. Lambrecht, and B. Segall, Phys. Rev. B **60**, 8087 (1999).
[36] D. A. Roberts, IEEE J. Quantum Electron. **27**, 142 (1992).
[37] S. K. Kurtz, J. Jerphagnon, and M. M. Choy, in *Numerical Data and Functional Relationships in Science and Technology*, edited by K.-H. Hellwege and A.M. Hellwege, Landolt-Börnstein, New Series, Group III, Vol. 11 (Springer, Berlin, 1979), p. 671.
[38] A. G. Jackson, M. C. Ohmer, and S. R. LeClair, Infrared Phys. Technol. **38**, 233 (1997).